applied sciences

MDPI

Article

Quantum Mechanical Coherence of K^+ Ion Wave Packets Increases Conduction in the KcsA Ion Channel

Johann Summhammer [1,*], Georg Sulyok [1] and Gustav Bernroider [2]

[1] Atominstitut, Technische Universität Wien, Stadionallee 1, 1020 Vienna, Austria; georg.sulyok@gmail.com
[2] Department of Biosciences, Universität Salzburg (retired), 5020 Salzburg, Austria (retired); Gustav.Bernroider@sbg.ac.at
* Correspondence: johann.summhammer@tuwien.ac.at

Received: 3 June 2020; Accepted: 18 June 2020; Published: 21 June 2020

Abstract: We simulate the transmission of K^+ ions through the KcsA potassium ion channel filter region at physiological temperatures, employing classical molecular dynamics (MD) at the atomic scale together with a quantum mechanical version of MD simulation (QMD), treating single ions as quantum wave packets. We provide a direct comparison between both concepts, embedding the simulations into identical force fields and thermal fluctuations. The quantum simulations permit the estimation of coherence times and wave packet dispersions of a K^+ ion over a range of 0.5 nm (a range that covers almost 50% of the filter domains longitudinal extension). We find that this observed extension of particle delocalization changes the mean orientation of the coordinating carbonyl oxygen atoms significantly, transiently suppressing their 'caging action' responsible for selective ion coordination. Compared to classical MD simulations, this particular quantum effect allows the K^+ ions to 'escape' more easily from temporary binding sites provided by the surrounding filter atoms. To further elucidate the role of this observation for ion conduction rates, we compare the temporal pattern of single conduction events between classical MD and quantum QMD simulations at a femto-sec time scale. A finding from both approaches is that ion permeation follows a very irregular time pattern, involving flushes of permeation interrupted by non-conductive time intervals. However, as compared with classical behavior, the QMD simulation shortens non-conductive time by more than a half. As a consequence, and given the same force-fields, the QMD-simulated ion current appears to be considerably stronger as compared with the classical current. To bring this result in line with experimentally observed ion currents and the predictions based on Nernst–Planck theories, the conclusion is that a transient short time quantum behavior of permeating ions can successfully compromise high conduction rates with ion selectivity in the filter of channel proteins.

Keywords: potassium ion channel; KcsA channel; selectivity filter; quantum wave packet; coherence time; biological quantum coherence

1. Introduction

Electrical signals generated in nerve cells are generated by membrane proteins that catalyze a selective electro-diffusion of ions across plasma membranes. The proteins are embedded in the lipid bilayer of membranes and provide currents at the pico-ampere level, combining fast conduction with a high selectivity for particular ions. In voltage-gated potassium channels, this selective control of ion conduction is organized by a specific arrangement of amino-acids within a narrow 'selectivity filter' domain of the protein [1,2]. The most frequently studied filter model is based on the bacterial-derived KcsA channel motif (KcsA, potassium crystallographically sited activation channel) where the filter

constriction is formed by four subunits, each composed by the same amino acid sequence TVGYG [3–5]. Ion translocation is largely coordinated by amino acid carbonyl groups pointing towards the axis of the constriction, with oxygen lone pair electrons creating a series of four potential valleys. By convention, and as shown in Figure 1, these transient cages are labeled as sites S1 to S4 as seen from outside to inside of the membrane with coordinating interactions mimicking the hydration shell of ions in bulk water [6]. The relevant caging forces are Coulombic attractions between ion and electrons, together with repulsive effects, if lone pair electrons and the inner shell of the K^+ ion start to overlap [2,6]. Further, the diffusion of K^+ ions seems to occur in a hopping manner between potential minima, and this in turn is driven by the transmembrane field resulting from the charge concentration gradient across the cell membrane. Additional to K^+ ions, also water molecules diffuse through the channel, experiencing similar carbonyl-derived caging forces.

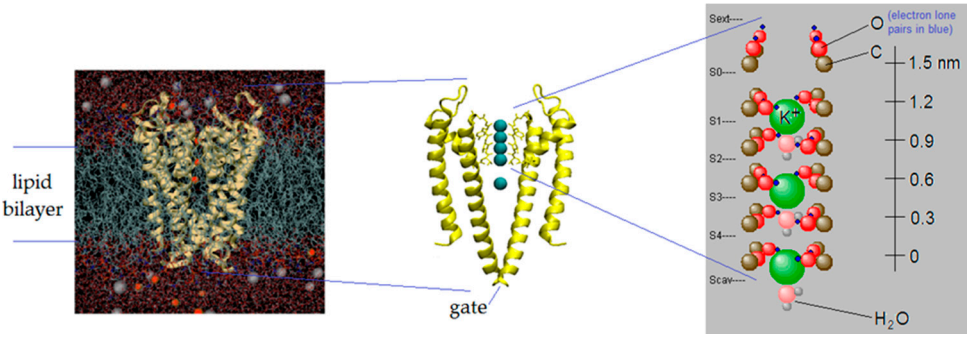

Figure 1. A ribbon model K^+ channel embedded in the lipid bilayer (**left**), with two of the four subunits and the extracellular side on top (**middle**). The four binding sites (S1–S4) with four dehydrated ions in locations S1 and S3, and one partially dehydrated ion in the neighboring cavity location S_{cav}, are demonstrated (**right**). Ions are kept in green color, water is shown in pink, carbonyl oxygens in red, and backbone carbon atoms in brown color. Lone pair electrons attached to oxygens are indicated by blue dots. The close-up view on the right side sketches the relative sizes of particles, which are assumed to be as follows: ion radius of K^+ =138 pm; covalent radius of carbon (when in double bond with O)= 64.1 pm; covalent radius of oxygen (when in double bond with C) = 58.9 pm; center–center distance of C and O-atoms in carbonyls = 123 pm; H_2O: covalent radius of O-atoms 73 pm; bond radius of H-atoms = 38 pm; center–center distance between O and H= 95.84 pm.

The small interaction distances of temporary caging sites together with the underlying conduction strategy, as hopping from one site to the next, stimulate the question of whether quantum effects in these transitions could play a functional role. In a recent study we have provided a first assessment of this question by simulating a single site situation and simulating a K^+ ion as a quantum mechanical particle. We found that, due to the slow dispersion of the initially well-localized wave packet, the enclosing carbonyl oxygen atoms tend to be pushed some distance aside, and this leads to a higher probability for the particle to escape from this site within a given time [7]. In the present work, we extend this study to include the complete TVGYG sequence and permit an arbitrary number of K^+ ions and water molecules to permeate. Again, we find a considerable enhancement of a K^+ ion's probability to propagate to the next site due to its quantum mechanical nature as a wave packet. Further, the present study confirms our previous finding about an optimal decoherence time of the particles' wave-function regarding a directional 'guidance' through subsequent potential barriers provided by the surrounding electrons.

Previous studies were generally based on classical MD simulations. Whereas early studies within this frame considered an alternating sequence of K^+ and water molecules (e.g., KwKw) passing through the constriction [4], subsequent MD simulations also revealed other conduction mechanisms with similar free energy barriers [8] and (Kw) co-translocations [9]. In addition, for high conduction rates, a direct Coulomb knock-on mechanism was suggested with direct ionic contacts [10]. A particularly important observation that strongly encouraged the present study was the observation about the

height of mean potential barriers that, at a temperature of 300 K, can be expected to be above 5 kT. With these kinetic barriers separating ions, the experimentally observed conduction rates cannot be explained [11]. The model presented here, however, offers an explanation for this observed discrepancy, demonstrating how high potential barriers can compromise with high conduction rates if the ion's behavior is described by quantum mechanical methods.

2. Materials and Methods

2.1. General Methods

In the present simulation, both the classical and the quantum mechanical diffusion of K^+ ions were based on an identical physical structure providing the ion environment. As seen from the intracellular site, the selectivity filter (SF) of the potassium channel had a narrow constriction of about 1.5 nm in length through which the ions had to pass prior to exiting the channel protein. The effective diameter of this domain was within the range of the electron shell diameter of K^+ ions, implying that any interaction with surrounding electrons is basically a quantum physical phenomenon. The channel model we applied was the same as in our previous studies and demonstrated on the right side of Figure 1 [12,13]. The 'binding sites' for dehydrated K^+ ions were designated as S1–S4, as seen from outside the cell with additional locations at the extracellular site (S0) and the internal channel cavity S_{cav} for fully or partially hydrated ions. As in most simulations, we kept the backbone atoms of the alpha-helices lining the filter at fixed positions, but we allowed for their carbonyl groups oriented towards the pore axis to change their vibrational motion. Each oxygen atom of a carbonyl (oxygens are shown as red spheres) has a constant distance to its carbon, but it can vibrate around its mean position in both angular directions. The carbon atoms have a positive partial charge, and the oxygen atoms have a negative partial charge of equal magnitude. Whereas the charge of a carbon atom is centered at this location, the charge on the oxygen is dispersed representing oxygen lone pair electrons. Non-shared oxygen lone pair charges are considered to play an important role in coordinating and guiding K^+ ions and water dipoles during diffusion through the narrow SF constriction atoms. We initially located these charges along an extension of the C=O binding axis and implemented carbonyl angle-bending modes in dependence of ion location.

The mobile species in the SF are K^+ ions (green spheres) and water molecules (pink oxygen atoms and attached grey hydrogen atoms in Figure 1). Ionic motion can occur bidirectionally along the SF central axis. Water molecules carry partial charges that compensate in sum but carry an electric dipole moment with two opposing axis orientations and arbitrary rotational orientation.

2.2. Classical MD Simulations

From a geometrical perspective, the variation of ion coordination is strongly confined to the axial extension of the filter domain (z-axis), and it can be safely assumed that lateral motion is negligible. This aspect also reduces computational efforts significantly. Furthermore, to achieve the present intention to compare a classical with a quantum mechanical interpretation of ion motion, the classical environment had to be designed in a way that subsequently allowed the extension to a quantum algorithmic implementation. This view necessitates a special implementation of force fields and in our case a computational design based on Verlet's algorithm [14]. We calculated the force between any two particles A and B, consisting of a Coulomb attractive and of a repulsive part, as follows:

$$F(r_A, r_B) = -\frac{1}{4\pi\varepsilon_0}\frac{q_A q_B}{(r_A - r_B)^2}\hat{r}_{AB} \quad \text{if } |r_A - r_B| \geq d_{AB} \tag{1}$$

and

$$F(r_A, r_B) = -f_{rep,AB}\hat{r}_{AB} \quad \text{if } |r_A - r_B| < d_{AB} \tag{2}$$

Here, ε_0 is the dielectric constant of vacuum, r_A and r_B are the position vectors of particles A and B, respectively, and q_A, q_B are their respective electric charges. The unit vector $\hat{r}_{AB}$ points from A to B, so that $F(r_A, r_B)$ describes the force that particle B exerts on A, and for the inverse we set $F(r_A, r_B) = -F(r_B, r_A)$. If the two particles get closer, beyond a critical distance d_{AB}, which depends on the type of their combination, the particles start to experience a constant repulsive force of positive magnitude $f_{rep,AB}$. In standard MD models, as those building on AMBER, CHARMM, or similar force fields [15], one would employ Lennard–Jones-type repulsion/attraction terms to incorporate dispersion and van der Waals forces. The present focus, however, was laid on a comparable quantum to classical situation, implementing some computational simplifications, e.g., setting some of the force field variables to constant values. A list of these values for $f_{rep,AB}$ and d_{AB} and for the various combinations of particles is given in Table A1. For water molecules, the total force experienced acts on its effective charge center, thereby avoiding torque. This also applies to the repulsive force in case of overlap of electron shells with an O-atom, a K^+ ion, or another water molecule.

The present simulation builds on the open-gate structure of the channel with ionic access to the channel cavity and filter domain. Upon entry to the filter, restriction ions are dehydrated replacing water complexation with carbonyl derived charges of the filter. This process is assumed to be initiated by the partial pressures of K^+ and H_2O, so that on average the particle current of both species is the same in accord with empirical and theoretical findings [9,16]. It should be mentioned that not all theoretical models agree on this point [10] (see discussion). Pressure at the atomic resolution is expressed by the frequency and strength of thermal contacts among particles along the axial direction. Across the four filter sites S4–S1, ions can be transiently bound, depending on random fluctuations of carbonyl atoms which connect the SF to the back bone atoms' thermal bath. In particular, carbonyl O-atoms are not only subject to forces exerted by other particles modeled in Figure 1 (right image), but in addition they also experience a dissipating force which is proportional to their fluctuation velocities. Dissipation in essence leads to an energy transfer to backbone atoms of the alpha-helix. Carbonyls are also exposed to a random force included at each time step of the present calculation, keeping the average vibrational motion of carbonyls to the level expected at 310 K. Carbonyl O-atoms in turn convey this random motion to K^+ ions and filter H_2O molecules. Occasionally this random motion reaches up to a strength that provides sufficient energy for a K^+ ion to cross the potential barrier from one site to the next. With H_2O molecules, the partial charges on the carbonyls do not provide the same coordination strength as seen for K^+ ions, basically easing the translocation of water through the SF. However, as H_2O molecules generally follow and line up with K^+ translocation [9], water flow on average seems to mimic K^+ currents. Overall, we find that ion currents resolved at the pico-second time resolution are largely characterized by a stop-and-go motion with long time intervals between transitions and flushes of conduction during short time intervals. Further details of the present MD model and specific parameters are given in Appendix A.

The present classical approach resolved in a stepwise implementation can be summarized by the following sequence of settings: Initially, four K+ ions and four H_2O molecules were placed within the SF in alternating sequence and are assumed to have some velocities between 200 and 300 m/s, i.e., velocities that are to be expected from a Maxwell–Boltzmann distribution at 310 K. Carbonyl O-atoms set out from their equilibrated positions and vibration. Subsequently, the dynamical evolution, implemented by Verlet's algorithm, was initiated with a run for 4 ns. This time frame is sufficient to reach thermal equilibrium. Following thermal equilibration, simulation runs were initiated covering time ranges between 1 and 10 µs, and with each run resolved into short periods of 20 ps. Each final configuration of these periods delivered the initial configuration of the subsequent period with Verlet time steps set to 0.25 fs. During a run, the time of emission of a K^+ ion was registered, and, optionally, a graphical image of the whole configuration of particles at the end of 20 ps was recorded. From these data the general behaviors of K^+ and H_2O flows through the SF and various statistics can be obtained. Additional technical details of the runs are given in Appendix A. Short videos of such runs are available as Supplementary Material.

2.3. Quantum Mechanical Simulations

In quantum mechanical (QM) simulations, one of the K^+ ions evolves as a QM wave packet, whereas other particles continue to be treated in a classical way, with forces given by Equations (1) and (2). The action of the classical particles on the quantum particle is described by an appropriate potential. The reverse action however, exerted by a quantum particle on a classical particle, requires modification of Equations (1) and (2). This modification reflects the typical quantum effect of a dispersion derived from a probability distribution as it emerges from Schrödinger equation.

If we denote the position of the quantum mechanical K^+ ion by the vector r, and its charge by q, then integrating the force as given by (1) and (2) provides the potential induced by a classical particle at r_B:

$$V(r, r_B) = \frac{1}{4\pi\varepsilon_0}\frac{qq_B}{|r - r_B|} \quad \text{if } |r - r_B| \geq d_{AB} \tag{3}$$

and

$$V(r, r_B) = f_{rep,AB}\cdot(d_{AB} - |r - r_B|) \quad \text{if } |r - r_B| < d_{AB}, \tag{4}$$

where d_{AB} is defined as in (1) and (2). Now, the Schrödinger equation for the ion can be written as

$$\left[-\frac{\hbar^2}{2m_K}\frac{d^2}{dr^2} + \sum_j V\Big(r, r_j(t)\Big) + V_{lin}(r)\right]\psi(r,t) = i\hbar\frac{\partial}{\partial t}\psi(r,t). \tag{5}$$

In (5), m_K denotes the mass of the K^+ ion, and the summation 'j' is carried out over all classical particles. The potential $V_{lin}(r)$ accounts for the overall linear gradient caused by the imposed transmembrane potential at the location of the channel. Solving the above equation is challenged by the fact that the wave function representing the position distribution of the ion $\left|\psi(r,t)\right|^2$ acts back on all classical particles modifying their positions $r_j(t)$. As a result, $V\Big(r, r_j(t)\Big)$, at a given time t, is determined by $\psi(r,t)$ over the entire position space. This effect introduces a more difficult non-linearity into the above model. We find, however, that the phase of $\psi(r,t)$ changes considerably faster as compared to $V\Big(r,\ r_j(t)\Big)$, and under this condition Equation (5) can be solved in a stepwise manner. During each step, classical particles are 'frozen' for short intervals τ_{cl}, and during these intervals the quantum mechanical evolution can proceed in the usual linear way. For this linear evolution we employed the numerical Crank Nicolson method [17]. After each interval τ_{cl} the resulting position distribution $\left|\psi(r,t)\right|^2$ serves to determine the new positions r_j that can be expected during the next interval τ_{cl} due to the action of classical forces proportional to $\left|\psi(r,t)\right|^2$. The resulting potential $V\Big(r, r_j(t)\Big)$ is finally inserted into Equation (5) to calculate the evolution of $\psi(r,t)$ during the next interval. The interval τ_{cl} is equivalent to a Verlet time step of purely classical MD simulations (usually at 0.25 fs), whereas the time step for the numerical solution of (5) by the Crank Nicolson method was kept to $\tau_{cl}/100$.

It seems to be important to understand the effect of back action of the wave function on the position of classical particles. This requires an additional inspection of the engaged forces. Equations (1) and (2) have to be modified to provide the force between a point particle and a dispersed QM K^+ ion, requiring that integration has to be extended over the entire domain of the dispersed ion. Keeping in line with Equations (1) and (2), we set r_A and q_A again to denote position and charge of the QM K^+ ion in focus:

$$F(r_A, r_B) = -\frac{q_A q_B}{4\pi\varepsilon_0}\int \frac{\left|\psi(r_A,t)\right|^2}{|r_A - r_B|^2}\hat{r}_{AB}\cdot dr_A \quad \text{for the domain } |r_A - r_B| \geq d_{AB} \tag{6}$$

and

$$F(r_A, r_B) = -f_{rep,AB}\int \left|\psi(r_A,t)\right|^2\hat{r}_{AB}\cdot dr_A \quad \text{for the domain } |r_A - r_B| \geq d_{AB} \tag{7}$$

These integrals were solved numerically by summation over the relevant range of $\psi(r_A,t)$ resolved into 1500 to 2000 increments along r_A for each interval τ_{cl}. Further details of the quantum mechanical calculations are given in Appendix A.3.

3. Results

3.1. Classical MD Simulations

In the KcsA model, conduction is estimated to reach up to maximal currents in the order of 10^8 ions per second [16,18]. The present MD simulations can basically reproduce this result. At the single-atom scale, however, conduction appeared to follow a quite different temporal characteristic than one would expect from electro-diffusion based on continuum Poisson–Nernst–Planck (PNP) models. Here we found that, on average, an ion was transmitted only every 2 to 5 nanoseconds to the extracellular domain. Together with average occupancies of the filter between 2 and 4 ions, an ion was found to spend between 6 and 15 ns in the SF domain. Translocation between binding locations within the filter were very short and occurred within around 1 picosecond crossing distances of 0.3 nm between each site. One could expect that ions can transverse the entire SF within 5 to 10 picoseconds, but the present simulations indicated that, on average, it took about 1000 times longer compared with this theoretical option. The reason can be found within strongly extended halting times that are largely suppressed in the macroscopic approximation of a continuous ion flow. At the present scale, sub-molecular details explicit the coordination strength exerted by surrounding carbonyl charges [19]. As a result from this Coulombic coordination, currents showed a temporal substructure in which consecutive bursts of ions were interrupted by exceedingly long intervals during which no ions left the SF. Figure 2 shows the result of a simulation which covered a period of 10 µs. During this interval, 1763 K^+ ions left the SF to the extracellular side. Although the average time between ion emissions is expected to be around 5.67 ns, more than 89% of the ions exited the SF within less than 2 ns of the previous emission. The above findings demonstrate a strong bursting characteristic, if the process is resolved to the highest level at the single-atom scale. In accord with this finding, there was a strong discrepancy between predictions based on a simulated Poisson-type (P) behavior and the present findings. As apparent from Figure 2, a sequence of 1763 random P events was compared to the emission characteristic following from our simulation.

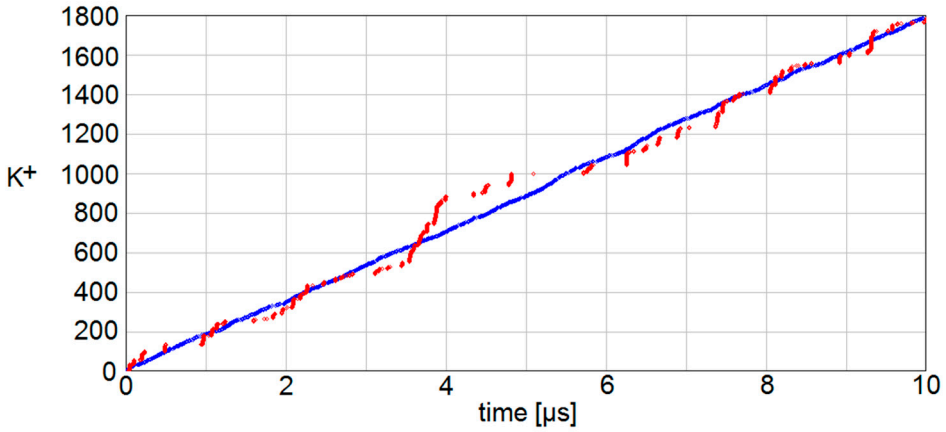

Figure 2. Red dots: Classical MD simulation of K^+ current through the SF during 10 µs; 1763 K+ ions left the SF at the extracellular side, mostly in bursts with very short time between successive ions. Blue dots: A mathematical sequence of random events according to a Poisson statistic which was set to produce a mean of 1763 events in 10 µs.

Finally, as seen from a 'classical perspective', the present results render a picture on the question of optimization of selective conduction, which has been at the focus of debate in previous studies. Details of these results will be published separately [20]. In short, changes in critical measures such as the length of the filter region had a strong effect on conduction. Changes of just a few percent (e.g., 4%) will halve conduction, and changes around 10% will freeze conduction completely.

The optimum length of the SF seemed to be about 0.7% longer than the values we assumed for the present calculations.

3.2. Quantum Mechanical Motion of a K^+ Ion

3.2.1. Coherence of the Wave Function

At absolute zero temperature (0 K), the wave packet of the K^+ ion maintains its coherence permanently. In this idealized situation, all interactions between the ion's wave packet and the atomic structure of its surrounding would evolve in a completely deterministic way. However, since the ion is exposed to physiological temperatures, the surrounding thermal bath is subject to random interactions between ions and the backbone atoms of the filter. The evolution of the ion wave function obtains a random element. Eventually, there is a loss of coherence between different spatial regions of the wave packet and a quantum–classical transition is initiated. It seems to be important to obtain estimates about coherence time τ, which is the typical time it takes until coherence is lost to a significant degree. The loss of coherence generally follows an exponential decay law [21], and if we set the maximum of coherence to 1, this can be seen as

$$C(t) = e^{\frac{-t}{\tau}} \tag{8}$$

Empirically, coherence time τ can be estimated in the following way. First a classical MD simulation is initiated where several K^+ ions enter and leave the selectivity filter until a specific configuration of K^+ and H_2O particles is found after some time interval t_{start}. Following this initiation, a K^+ ion is selected for QM simulation, and this simulation is continued over some time interval Δt during which the chosen K^+ wave function evolves quantum mechanically according the Schrödinger equation. All other particles behave classically, as before. The evolution of the QM wave function is recorded, and the conditions at time t_{start} are stored. Following this step, the evolution during time interval Δt is repeated. This time, due to random perturbations from the thermal bath, the particle wave function follows a slightly different path. The two emerging versions of the wave partly overlap giving rise to interference terms, similar to the situation expected from a double-slit experiment [22]. Finally, the normalized magnitudes of this interference provide an estimate for coherence. Figures 3 and 4 provide a typical example for this situation. Figure 3 shows the real part of the wave function at the beginning and after 0.5 ps for two separate evolutions of the wave function. Figure 4 provides the coherence terms of two such separate evolutions during an interval of $\Delta t = 1$ ps.

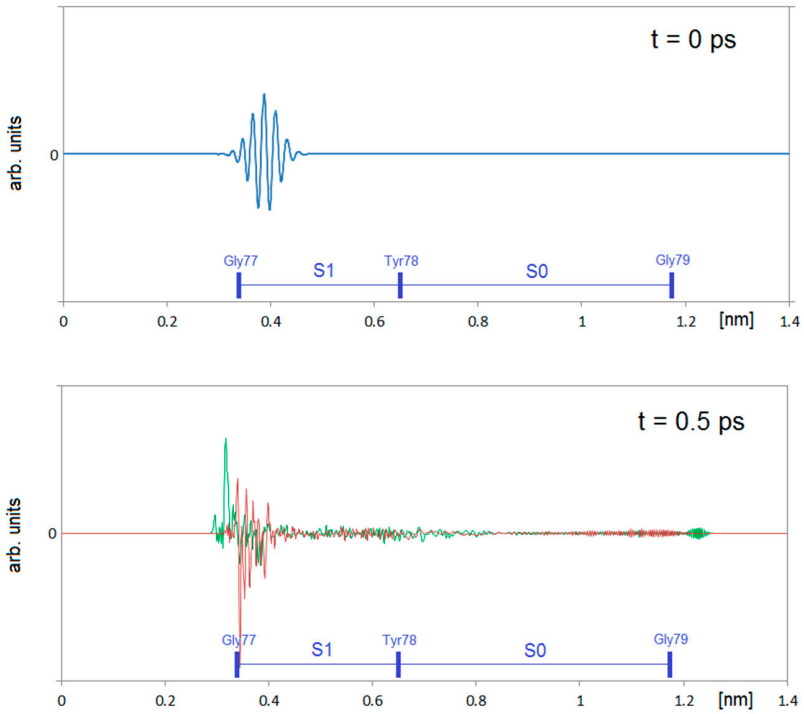

Figure 3. Top: Real part of the wave function at the beginning of the quantum mechanical calculation.

The length of one oscillation corresponds to the mean de Broglie wavelength given by the mean momentum of the K^+ ion. (Since the particle starts as a localized Gaussian wave packet, it actually contains a wide spectrum of de Broglie wavelengths.) The particle is on the lower side of site S1 (see, e.g., Figure 5a). The blue scale near the horizontal axis shows the range of sites S1 and S0, as defined by the charge centers of the respective lone pairs of the oxygen atoms of the carbonyl groups of Gly77, Tyr78, and Gly79, respectively. **Bottom**: Real part of two separate evolutions (one red, one green) of the wave function after 0.5 ps, which happened under identical conditions except for random thermal noise introduced by the oxygen atoms of the carbonyl groups. The mean positions are already slightly shifted. In both cases, a significant part of the wave function extends over almost one nanometer and reaches over more than two sites.

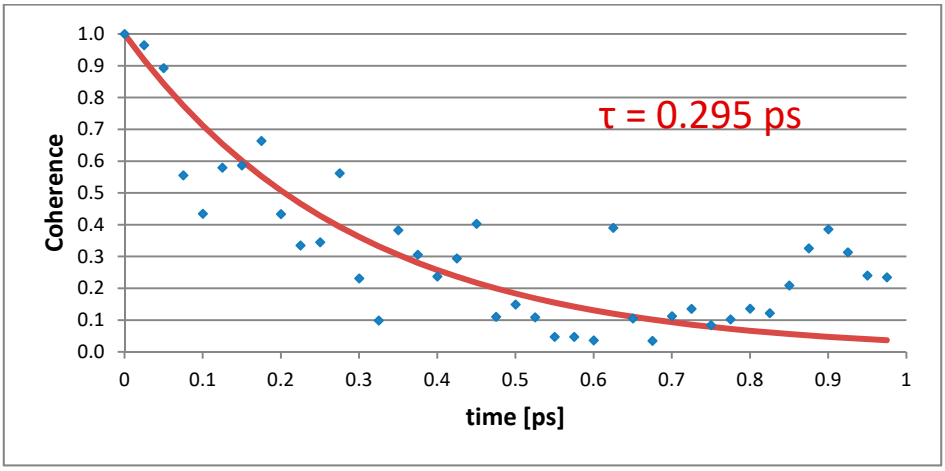

Figure 4. Example of decreasing coherence due to thermal perturbations. Results from a simulation are shown as blue crosses. The red line provides a least-squares fit of Equation (8) to the observations, giving a coherence time of 0.295 ps. A detailed explanation how coherence was calculated is given in Appendix A.4.

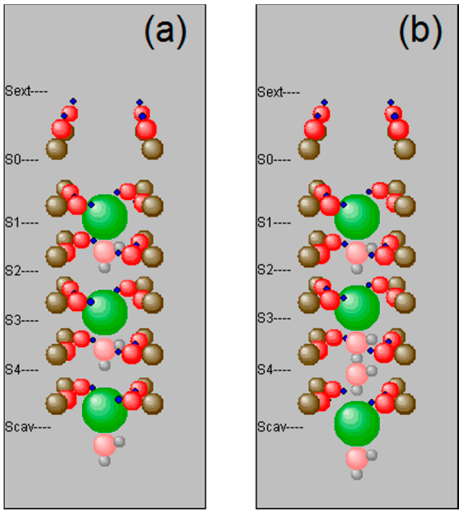

Figure 5. The two configurations (KWKWK) (**a**) and (KWWKWK) (**b**) as seen from inside to outside of the filter which caused the longest non-conductive state in the classical MD simulations.

As can be seen form the inserted examples, coherence terms are subject to perturbations from oxygen atoms adding random phases to the evolving wave function. A least-squares fit to the present data yielded a coherence time of 0.295 ps in the cases shown and can be expected to lay between 0.1 and 0.3 ps. In addition, coherence decay did not seem to follow a strict exponential law, but long-lived tails rendered some significant coherence after more than 1 ps. This observation is in good agreement

with previous estimates [23] but is somehow shorter compared to other reports providing estimates of several tens of picoseconds as in [22].

3.2.2. The Effect of QM Coherence on K^+ Conductance

As has been found in classical MD simulations, the K^+ current through the selectivity filter consisted of a series of bursts with long, intermittent halting periods reaching up to several hundred nanoseconds (Figure 2); again, these halting periods are characterized by some typical configurations of K^+ and H_2O particles. Figure 5 demonstrates two such examples. As before, the most stable configurations were S1–0–S3 or with an intermittent water S1–W–S3.

A break up of this situation can occur if the K^+ ion in site S1 moves up to the next potential valley. In this situation, particles from the lower positions can follow, and this leads to vacancies for additional ions to enter the selectivity filter from the inner cavity. This observation opens the question whether a quantum mechanical treatment of the K^+ ion at site S1 in such a configuration can predict shorter halting periods and, thus, an enhanced K^+ current. Signatures for this to occur are indicated by the evolution of the wave packet as shown in Figure 3. For the time t = 0.5 ps, both examples of wave evolutions show an appreciable probability amplitude of the K^+ ion in a region well beyond the carbonyl oxygens of Tyr78 located at around 0.65 nm. This indicates some possibility that the K^+ ion can also be found at site S0 at this very instance of time. In the classical situation the ion has to remain at site until a peak in oxygen vibrational motion provides the force for transition. Opposed to the classical situation in the QM version there are at least two reasons why the wave packet can propagate more easily into site S0. One reason is tunneling [24]. The other reason, which we have suggested in a previous report [7], is that the front part of the wave packet drags the oxygen atoms upward, reducing the confining potential for the lower part of the wave function, which can then propagate more easily.

At this stage it cannot be said with certainty which of the two strategies will dominate, but evidence from previous calculations, as presented in [7], is strongly suggestive for the second option. In order to estimate the transition time of the ion to site S0, we inspected the probability distribution that emerged in course of decoherence.

Let $W_z(t)$ be the probability to find the particle above a certain position z at time t as calculated from a non-decohering wave function. Our interest focuses on positions z in the range of site S0. If coherence time is τ, then the probability for the wave function to lose coherence within an interval dt is given by

$$p_{inc}(t)dt = \frac{e^{-t/\tau}}{\tau}dt \tag{9}$$

The average probability P_z, to find the K^+ ion after decoherence at locations above z is then given by

$$P_z = \int_0^\infty p_{inc}(t)W_z(t)dt. \tag{10}$$

At this stage we recall that the environment of ions acts as a detector for the positional degree of freedom of ions within a temporal scale provided by coherence time. Over a longer period of time, the evolution of an ion is composed from a series of short quantum evolutions with random moments of decoherence. Each formation as a new wave packet at a new position will of course satisfy energy and momentum conservation. Consequently, it is the location of the ion at the moment of decoherence which becomes decisive for the further development of its wave function. Should this location be above the threshold z we expect its translocation within one coherence interval τ. If this location happens to be below the value of z, the particle's wave function has to evolve again setting out from the initial location. If after two attempts the particle translocates, we assign a transition time of 2τ. Considering all possibilities, the mean time $\overline{T}$ for translocation from site S1 to site S0 can be seen in the polynomial

$$\overline{T} = \tau{\cdot}P_z + 2\tau{\cdot}P_z(1-P_z) + 3\tau{\cdot}P_z(1-P_z)^2 + \ldots = \tau{\cdot}\sum_{n=1}^{\infty} nP_z(1-P_z)^{n-1} = \frac{\tau}{P_z}. \tag{11}$$

3.3. Temporal Characteristics

At first sight, (11) would predict an increase of $\overline{T}$ with increasing coherence times. However, there emerges a characteristic quantum effect strongly influencing the pattern behind time $\overline{T}$. If τ is very small, the quantum wave packet exists only for a very short time and small spatial spread, so that the probability P_z for extending into the next site is also small (e.g., initial expansion terms are quadratic in time). As a result, time $\overline{T}$ is extended and coherence time τ is small, the situation approaching a classical situation. However, halting time $\overline{T}$ can also be large with long coherence times as P_z converges to a value determined by the height of the separating potential barrier between two neighboring sites. As a result, we observed halting time $\overline{T}$ passing through a minimum when P_z was still rising for intermediate values of coherence time. In most instances this minimum was reached when τ acquired typical values for K^+ ions in the SF, which was around a few tenths of a picosecond (Figure 4).

In order to see how this quantum phenomenon could change the conductance of K^+ ions through the selectivity filter, we compared the situation with classical MD simulation over a period of 660 ns and recorded the time of each emission of a particle simultaneously with the alignment of filter occupations of ions and waters. Within one series of runs a total of 218 K^+ ions were emitted, and roughly the same number of H_2O molecules. The two configurations which produced the longest halts of current are shown in Figure 5. For these two configurations we again simulated runs in which the top K^+ ion was represented as a quantum mechanical wave packet. Short period (2 ps) time intervals were repeated many times to yield estimates of coherence and halting times prior to a transition from site S1 to S0. We found that during the 660 ns of MD simulation, the configuration shown in Figure 5a occurred three times, and the corresponding halting times were 6.5, 21.9, and 87.4 ns, respectively. The average classical halting time was, thus, 38.6 ns. For the quantum mechanical simulations we selected four different starting times. For each situation we calculated a number of evolutions which differed in the width of the initial wave packet. These widths varied between 0.005 and 0.05 nm (defined as the width characterized by a probability density above 1/e of peak values). The evolution, which gave the longest halting time, was taken as the most credible one because it implied that with this width the wave packet had the smallest exponential penetration into the classically forbidden zones of the potential. We also calculated the halting times for different coherence times. We obtained an average halting time of 1.16 ns for a coherence time of 0.4 ps and of 10.16 ns for a coherence time of 0.1 ps. Therefore, even if we assume a relatively short coherence time of 0.1 ps, the quantum mechanical halting time was only around 25% of the classical one. The configuration in Figure 5b also occurred three times with halting times of 21.6, 47.7, and 236.1 ns, respectively, thus providing an average of 101.8 ns. Under the same conditions as above, we obtained an average halting time of 0.60 ns for a coherence time of 0.4 ps, and of 33.90 ns for a coherence time of 0.1 ps. For the shorter coherence, the halting time in the quantum case was now around 33% of the classical one. Figure 6 depicts the classical and the quantum mechanical evolution of a wave packet with an original width of 0.05 nm and the corresponding classical configuration at the beginning and after an elapsed time of 0.227 ps. One notes that the QM wave packet has already an appreciable presence within site S0.

Looking at the situation from a more conservative point of view by assuming coherence times around 0.1 ps, we also found a total gain in the comparison of the two configurations shown in Figure 6 of 290 ns in favor of the QM-MD simulation. This would amount to an almost 1.8-fold increase of the K^+ current due to quantum coherence. However, the present results also require a note of caution regarding two aspects. First, the present study cannot cover all possible configurations which may play a role for interrupting the ions flow. The second aspect refers to the specific location of the QM simulated ion. Here we focused on the top locations S1-S0 which provide a higher vacancy for channel emission compared to more central locations. More central locations of the filter might also involve opposite effects on halting times. Repulsive effects of the particle wave function in this case might lead to increased distances to other atoms, a situation known for example from the behaviour of free electrons in liquid helium. There the electron's wave packet can form a bubble of almost 4 nm in diameter which contains no liquid [25].

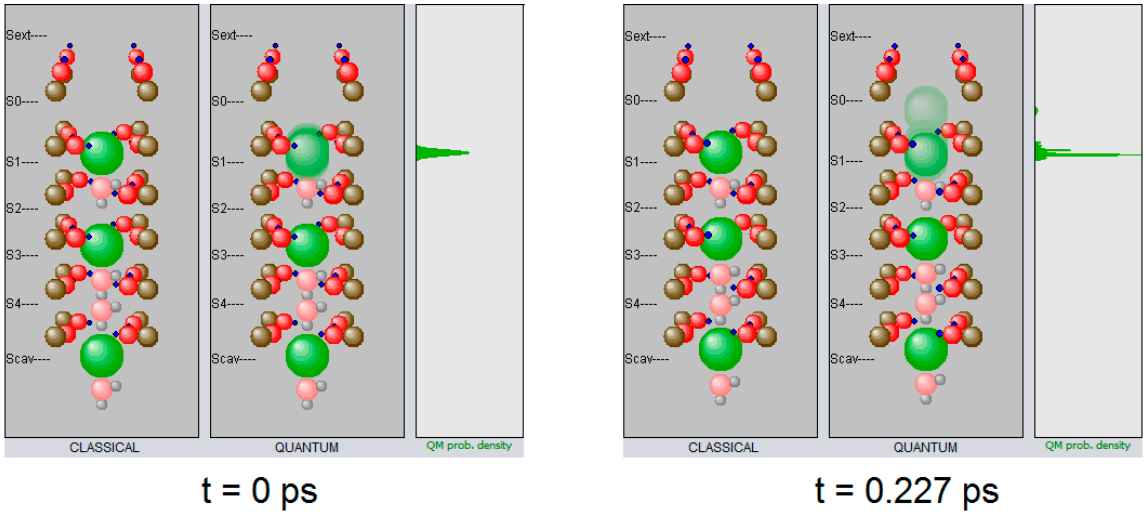

Figure 6. Configuration in the selectivity filter for time t = 0, when the evolution was started, and for time t = 0.227 ps, which is a typical coherence time for this configuration (see Figure 4). In each picture the classical case is on the left, the case with the topmost K^+ ion calculated as a quantum mechanical wave packet in the middle, and the quantum mechanical probability distribution of the ion on the right. (The quantum mechanically calculated K^+ is shown as partly overlapping semi-transparent spheres at different positions and the transparency scales inversely with the probability density at that position.) At t = 0 ps, the quantum mechanical ion has a certain spread due to the Heisenberg uncertainty. At t = 0.227 ps, this wave packet has gained a noticeable extension into the site S0. (An animation showing the entire evolution is available as Supplementary Material).

4. Discussion

Within the classical version of the present MD simulation, performed at the level of single atoms and at femto-second resolution, we have found a clear difference to predictions based on general Poisson statistics. Translocation of ions occurs in single bursts, separated by extended periods of no conduction that can extend over intervals of hundreds of ns (thus extending to the microsecond time scale). This highly irregular behavior can be found to be substantially caused by the coordination energy and barrier height imposed by lone pair charges of carbonyl oxygen atoms in accord with previous findings [2–4,6,8–10,26]. A K^+ ion can escape from these 'oxygen cages' if thermal fluctuations and oxygen vibrational modes occasionally exceed certain limits. This perturbation, in turn, exerts an agitation effect on all atoms of the selectivity filter and initiates a cascade of events, involving transitions of ions and water within the filter and new particles entering the filter domain from the core cavity. This later process then continues until the large vibrational amplitudes of the oxygen atoms subside by transferring energy into amino acid backbone atoms and K^+ ions can be captured again by the coordinating forces.

The quantum mechanical description of K^+ ion propagation indicates a different situation. This difference becomes especially noticeable if the ion configuration in the filter for a particular site is associated with a vacancy in the neighboring site directed towards the filters exit, e.g., between sites S1 and S0. In these situations, the coordination by the eight surrounding oxygen atoms is slightly weaker because the wave packet of the K^+ ion takes up more volume compared with a classical K^+ ion. This also applies for a wave packet at a minimum uncertainty. As the wave packet further evolves, it starts to spread into the unoccupied adjacent site by at least two mechanisms. One way is provided by 'normal leakage' exerted by high-momentum components present in any localized quantum particle, and involving energies higher than the separating barrier. The other possibility is quantum mechanical tunneling, whose non-negligible influence has recently been emphasized [24].

At this stage it is difficult to make predictions about the relative importance that both mechanisms will contribute to the QM phenomenon that we report. Whatever way may dominate, both processes

lead to a small but functionally significant presence of the particle's wave function in neighboring binding locations within one (or less) picosecond [7]. The extent to which this early probabilistic presence in the neighboring site leads to a real conduction event depends on the coherence time of the wave packet. Within a dissipative environment the wave packet will be re-created as a new and narrowly localized wave packet at coherence time scales. The place of this localization happens randomly, but with weights corresponding to the probability distribution at this moment. If coherence time is very short, there is little time for the wave packet to spread. The new localization can be expected to be localized primarily within the original site. As coherence time gets longer, the wave packet will spread more and can eventually reach into the neighboring site initiating some chance for the next localization to evolve at this new location. This is the point where an actual change in conduction can occur. In the present simulations, we found coherence times for a K^+ ion in site S1 to range between 0.1 and 0.4 ps with shorter times being more frequent. During such a short time, the wave packet would usually spread into site S0 with a weight between 10^{-5} and 10^{-3}.

Here we investigate the two configurations of K^+ and H_2O in the filter with the most extended non-conductive time intervals and with both configurations where a K^+ ion in located in S1 and a vacancy in S0. In both cases we found that the K^+ as a quantum mechanical wave packet can transverse from site S1 to site S0 in typically one-fourth to one-third of the time it takes a classical particle for the same transition. These results offer an important implication on a possible functional role of a quantum mechanical behavior for ionic transport in proteins. It predicts that ionic currents can be higher on the order of 1.8 times compared to an all-classical MD simulation. This gain in conductance also emerges if just one of the engaged ions is treated as a quantum particle in motion and potential barriers are unchanged, maintaining selectivity for the conspecific ion.

It is certainly an important question to what extent the predicted gain in ion currents is supported by physiological experiments. At the moment, this question cannot be answered with certainty because classical MD simulations, as well as the present quantum mechanical simulation of ion motion, are based on a choice of parameters shaping the potentials between the engaged particles. In both approaches, the involved parameters vary over certain ranges provided by other, e.g., structural considerations. It is a tradition to choose the set of electro-chemical parameters in a way that renders ion currents in agreement with the observed values. However, physiological observations provide conduction rates close to the diffusion limit of up to 10^8 ions/s. As was mentioned in the introduction, these physiological measures are at variance with the predictions from Nernst–Planck estimates and the potential barriers obtained by classical potential mean force estimates, e.g., [11]. The present simulation offers a way to explain these fast conductions without violating the barrier heights of more than 5 kT at 300 K necessary to maintain ion coordination and selectivity. Here we show that within a 'standard setting' the QM wave packet of an ion with the mass of a K^+ ion can spread beyond the width of a single coordination site of the KcsA filter domain during just a single coherence time interval. This is strongly suggestive that the underlying dynamics in the filter region of these ion channels involves an important quantum mechanical aspect. We expect that quantum properties become even more important if all ions occupying the channel are described as wave packets, as this will influence the mutual forces and will moderate the random fluctuations exerted by the atomic channel structure.

The present results suggest a number of future investigations. One topic to address is how the quantum mechanical behavior of a K^+ ion located at different sites of the selectivity filter will influence current flow, particularly within situations where adjacent locations are occupied by another ion, involving a direct Coulombic knock on. Another aspect involves the description of the K^+ ion employing a density matrix approach. Finally, we expect to gain further insight on the conspicuous burst-like behavior of current flow with all K^+ ions in the selectivity filter treated as quantum particles.

Supplementary Materials: The following supplements are available online: Video Seq1to12.mp4 (Link: https://owncloud.tuwien.ac.at/index.php/s/XkjnJhEpv78IEAK) and Video Seq13to24.mp4 (Link: https://owncloud.tuwien.ac.at/index.php/s/A66t6KxIhoNfKbi). Each of these two videos is composed of 12 clips of 20 ps duration, which show K^+ ions entering or exiting the selectivity filter and the motional re-arrangements before and after the events. Inserted comments explain the configurations and emphasize the long intervening intervals of no conduction.

Video CL-QM-comparison.mp4 (Link: https://owncloud.tuwien.ac.at/index.php/s/xGHNs1L2KANQvoZ). A film clip of 4 ps which compares the classical and the quantum mechanical evolution of a K^+ ion initially situated at site S1. Classically, the K^+ ion oscillates within S1 while quantum mechanically the wave packet also oscillates and simultaneously spreads into the range of S0.

Author Contributions: J.S.: formal analysis, software, data curation, visualization, writing—original draft preparation. G.S.: formal analysis, investigation, methodology, software, validation, writing—review and editing. G.B.: initialization, validation, conceptualization and writing—review and editing. All authors have read and agreed to the published version of the manuscript.

Funding: The authors acknowledge TU Wien Bibliothek for financial support through its Open Access Funding Program.

Conflicts of Interest: The authors declare no conflict of interest.

Appendix A

Appendix A.1. Numerical Parameters of the Particles and of the Selectivity Filter

The 'particles' involved in the MD simulations are K^+ ions, water molecules, and carbonyl groups. All particles were modeled as point particles carrying a partial charge and a typical radial extension where mutual repulsion would set in if any two particles were close. The K^+ ions carried a charge of +1 q_0, where q_0 is the electric unit of charge ($1.602176634 \times 10^{-19}$ Coulombs). The H_2O molecules were simulated as three separate charges located at the corners of a rigid triangle, and the usual parameters were assumed, i.e., an angle of 104.5° between the two arms to the H-atoms and a distance O-H of 95.84 pm. The partial charge on O was $-0.7\ q_0$ and that on each of the H-atoms was $+\ 0.35\ q_0$ [27]. In carbonyl groups the distance between C and O was set to the usual report of 0.123 nm. The C-atom carried a partial charge of $+0.38\ q_0$ [28]. The O-atom carried a partial charge of $-0.38\ q_0$ [28], of which 30% were located at the center point of the O-atom and 70% were located at an effective charge center, representing the lone pair electrons. (This distribution was estimated from trial and error to obtain the potential distributions as shown in [9] and [10].) The distance between the center of the O-atom and the lone pair charge point was set to 1.4 R_O, where R_O is the covalent radius of the O-atom when in double bond (58.9 pm). The lone pair charge point was always fixed on the extension of the C-O-line following the vibrational axis of the O-atom.

The dimensions of the selectivity filter were set by the fixed positions of the carbonyl C-atoms. We adopted values following Garofoli et al. [29]. For each amino strand, the C-atoms of the neighboring carbonyls had a constant distance to the central axis of the SF of 0.38 nm, and the four strands were arranged in a quadratic outline. Therefore, C-atoms of a given ring were located at corners of a square with side lengths of 0.5374 nm. The distances along the axis of the SF (*z*-axis) between the different rings were as follows: Thr74-Thr75 0.3 nm, Thr75-Val76 0.32 nm, Val76-Gly77 0.28 nm, Gly77-Tyr78 0.31 nm, and Tyr78-Gly79 0.35 nm. The orientations of the C-O axes in the relaxed condition point more or less to the central axis of the SF, although in most depictions of the KcsA filter one can find certain deviations [9,30,31]. For the present calculations the angles of the C-O axes were the same for each of the four carbonyls of a given ring, but could differ from one ring to the next. We set the angles as follows (φ ... angle in the xy-plane, a value of 0 indicates that C-O points to the central axis; θ ... tilt angle of C-O out of the xy-plane): At Thr74 $\varphi = +22.5°$, $\theta = 0°$; at Thr75 $\varphi = +22.5°$, $\theta = 0°$; at Val76 $\varphi = -22.5°$, $\theta = 0°$; at Gly77 $\varphi = +22.5°$, $\theta = 0°$; at Tyr78 $\varphi = -22.5°$, $\theta = 0°$; and at Gly79 $\varphi = 0°$, $\theta = 70°$. These orientations can be roughly inferred from the right image of Figure 1 (in this and all other figures of our model of the SF the lower ring is Thr74 and the top is Gly79).

Oscillations of carbonyl O-atoms with their relaxed values of φ and θ follow a linear Hooke's law in which the spring constant is set to result in a vibrational frequency with a wavenumber of 500 cm^{-1}. This is in the range of wave numbers established for carbonyl groups within similar molecular environments [32,33]. The damping constant of the vibration was set to 1×10^{-13} kg/s. This constant has only a small influence, however, because the connection to the thermal bath of the amino-backbone by means of random forces acting on O-atoms is dominant. This is in addition to the small oscillation amplitudes of 2–6 pm.

The box size of the simulation was $0.6 \times 0.6 \times 2.6$ nm. This box contained the 24 fixed carbon atoms, the 24 oscillating oxygen atoms, up to 4 water molecules, and up to 4 potassium ions. H_2O molecules and K^+ ions which left the box at the top were no longer tracked. H_2O or K^+ entering from below started to be tracked upon entry. The environment outside was not explicitly simulated but instead it was considered as a thermostat keeping the oscillating oxygen atoms at a mean energy corresponding to 310 K, together with any new H_2O or K^+ particles entering the box. In the numerical implementation of this Langevin-type thermostat, the O-atoms received a Gaussian-distributed random force input at every time step of Verlet's algorithm. The random force obeys the fluctuation dissipation theorem which keeps the O-atoms at the same temperature T as the surrounding environment. Newly entering H_2O or K^+ was given an initial velocity derived from a Boltzmann distribution at T = 310 K as well. The computer program for all simulations, the MD-part as well as the quantum mechanical part, was developed in-house from scratch, providing complete access to all aspects necessary for comparing the two different approaches.

Table A1. Distances d_{AB} between particles where constant repulsive forces set in, and magnitudes $f_{rep,AB}$ of these forces ($k_B = 1.38064852 \times 10^{-23}$ J/K Boltzmann constant, T = 310 K). Particle combinations in which one partner is a C-atom are not listed, as their electron orbitals cannot get close enough, and hence only the Coulomb force applies.

Particle A	Particle B	d_{AB} [pm]	$f_{rep,AB}$ (Units of k_BT/d_{AB})	Comment
K^+	K^+	-	-	Very strong Coulomb repulsion, no additional repulsion needed
K^+	O (central charge)	131	500	This repulsion hardly comes to play, because the K^+ remain on the central axis of the SF.
K^+	O (lone pairs charge)	248	100	Plays an important role for keeping a K^+ coordinated at a site.
K^+	H_2O	192.5	1000	Determines how close an H_2O can get attached to a K^+ while following it through the SF.
O (central charge)	H_2O	137.5	500	This repulsion hardly comes to play, because the H_2O molecules remain on the central axis of the SF.
O (lone pairs charge)	H_2O	137.48	350	Represents an occasional barrier for an H_2O to pass on, depending on how it is oriented.
H_2O	H_2O	137.5	500	The Coulomb force acts between the three charges of each H_2O. The distance for repulsion is given by the distance between the charge centers.

Appendix A.2. Additional Aspects about MD Simulations

In the present MD model, the SF was aligned with the inner cavity of the channel protein according to its standard crystal structure. Entrance to the filter with ions located within proximity of the carbonyl ring Thr74 of 0.5 nm and below this distance occurred by thermal pushes at the order of 50 events per picosecond. Following thermal agitations, a particle acquires a velocity in the longitudinal z direction derived from a Boltzmann distribution at T =310 K. By changing this kick rate, the effective pressure exerted from the inner cavity atoms can be changed. New particles can enter into the SF from below at any time step. On the extracellular side of the membrane, the effective pressure of H_2O molecules and K^+ ions was represented by a potential barrier of 20 k_BT at 0.54 nm above the carbonyl ring of

Gly79. A particle which passed this barrier was considered as emitted from the SF and was not tracked any further.

Appendix A.3. Additional Aspects of Quantum Mechanical Simulations

A typical quantum mechanical evolution applying to the present situation is demonstrated in Figure A1. The topmost K^+ ion was simulated as a quantum mechanical wave packet for a period of 1.5 ps. The z-range extended from 0.6571 to 2.1000 nm. This range was divided into 1597 equidistant points. The time interval was divided into 6×10^5 time steps of the Crank Nicolson algorithm. The potential confining the quantum wave evolution was reestablished at time steps of 100 by updating the positions of all the classical particles The width of the original Gaussian wave packet at t = 0 was 0.04 nm (a width within which the probability density drops to 1/e of the maximum value).

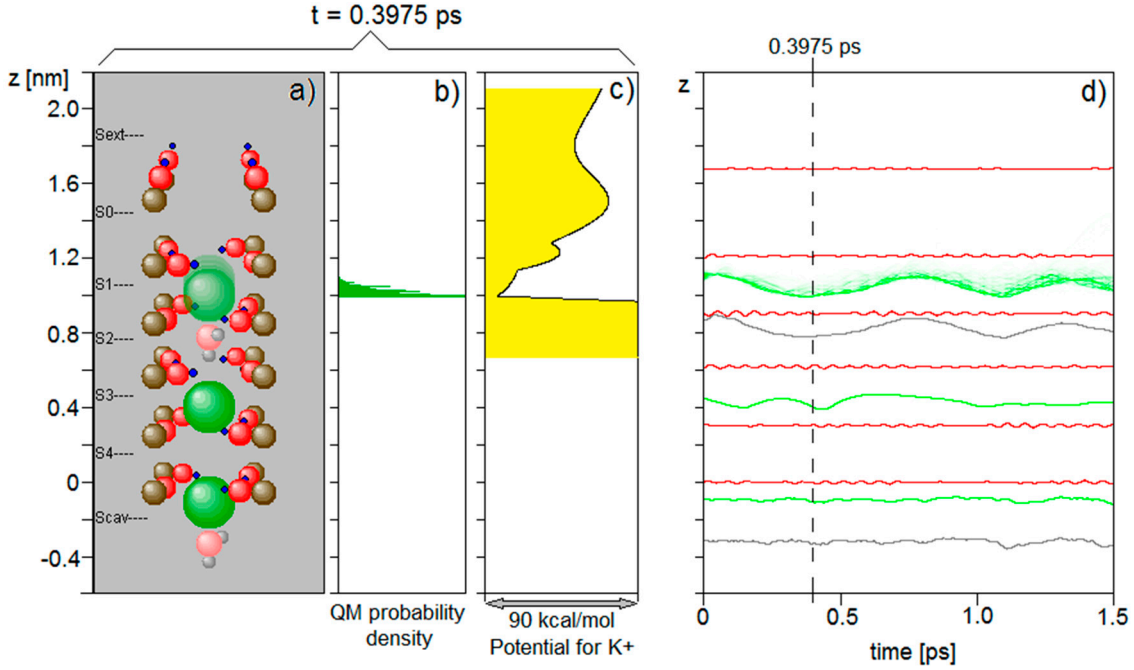

Figure A1. Snap shot of a quantum wave evolution at t = 0.3975 ps after initiation of the topmost K^+ ion as a Gaussian quantum mechanical wave packet (**a**–**c**) and z-coordinates of all particles as a function of time (**d**). (**a**) Configuration of the selective filter. The topmost K^+ ion is spread out; (**b**) quantum mechanical probability density along the *z*-axis of the mass center of the topmost K^+ ion at this instant of time; (**c**) potential to which the quantum mechanical wave packet is exposed at this moment of time. The yellow region is the range covered by the calculation. It extends beyond the region with appreciable probability to avoid artificial cut off effects. The K^+ ion wave packet is strongly confined to the lowest potential valley and is propagating back and forth within this region. In order for a significant escape it has to extend over the hill at z = 1.5 nm; (**d**) z-coordinates of the moving particles as a function of time. Green: K^+ ions, where the wave packet of the topmost ion is shown in shades corresponding to the probability density of location (darkest shade = highest probability density). Grey: water molecules. Red: oxygen atoms of the carbonyl groups. The dashed line indicates positions which are shown in the panels (**a**–**c**).

Comparing classical MD and quantum evolution. The entire procedure set out with a classical MD simulation which was also completely recorded. Upon viewing the evolution, a short time interval of interest covering at most 5 ps was chosen, and one of the K^+ presently in the selectivity filter was identified as the particle to be simulated as a quantum mechanical wave packet. Subsequently, the quantum mechanical simulation of the chosen time interval was started, in which all particles had the same initial positions and velocities as given by the classical version. For the

K+ ion simulated quantum mechanically, the mean velocity and mean position of the wave packet corresponded to the previous classical values. The initial width of the wave packet could be chosen freely, but above a certain minimal extension, because Heisenberg's uncertainty would also allow for energy components higher than the confining potential constraining a given site. This implies an initial wave packet width extending above a lower limit of about 0.02 nm. Following these choices, the calculation proceeded as outlined in Section 2.3, again recording its evolution. Finally, comparisons could be made as shown in Figure 6, and the collected data were processed into videos. The quantum mechanical simulation of 1 ps with a 2.5 atto-second time step takes less than 1 min on a 3.6 GHz i7-processor. The classical simulation of 20 ps with a 0.25 femtosecond time step takes about 0.8 s.

Appendix A.4. Coherence Calculation

According to the Schrödinger equation, the evolution of a wave packet of a K^+ ion within a time dependent potential caused by the motion of the surrounding oxygen atoms, water molecules, and other K^+ ions is always deterministic. This principle also applies if only a single realization of the random thermal fluctuations within the confining potential is considered. Since it has a definite form in time, one cannot expect the loss of coherence within a single evolution of a quantum mechanical wave packet because any two points in space of the wave packet will have a definite phase relation at every instant of time. The concept of (de)coherence can be defined only if multiple realizations of the thermal noise are accounted for. The same initial wave packet then evolves through the same temporal extension in a repeated way, and the potential exhibits a different random sequence of thermal fluctuations. In this case, the wave packets of different evolutions can be compared in a point-by-point manner for any chosen time. A signature of decreasing coherence is the observation that initially the wave packets overlap quite well, but as time continues the overlap reduces, e.g., as demonstrated in Figure 3, the overlap is perfect at t = 0 and has considerably decreased at t = 0.5 ps. This decrease of overlap indicates a decrease of coherence. However, for any two such wave packet calculations, this change of coherence is not necessarily continuously decreasing because it very much depends on the two particular realizations of the thermal random effects acting on the potential. This is shown in blue dots in Figure 4. However, if the wave packet evolves in a repeated way within the same time interval, and in addition the temporal pattern of the potential acquires a different random pattern, one finds that the mean value of coherence drops exponentially with time. This is reflected by the continuous function shown in Figure 4. The rate of its decrease defines the coherence time.

References

1. Hille, B. *Ion Channels of Excitable Membranes*, 3rd ed.; Sinnauer Associates: Sunderland, MA, USA, 2001.
2. Kuyucak, S.; Andersen, O.S.; Chung, S.H. Models of permeation in ion channels. *Rep. Prog. Phys.* **2001**, *64*, 1427–1471. [CrossRef]
3. Doyle, D.A.; Cabral, J.M.; Pfuetzner, R.A.; Kuo, A.; Gulbis, J.M.; Cohen, S.L.; Chait, B.T.; MacKinnon, R. The structure of the potassium channel: Molecular basis of K^+ conduction and selectivity. *Science* **1998**, *280*, 69–77. [CrossRef]
4. Morais-Cabral, J.H.; Zhou, Y.; MacKinnon, R. Energetic optimization of ion conduction rate by the K^+ selectivity filter. *Nature* **2001**, *414*, 37–42. [CrossRef]
5. Chattopadhyay, A.; Kelkar, D.A. Ion channels and D-amino acids. *J. Biosci.* **2005**, *30*, 147–149. [CrossRef]
6. Bostick, D.L.; Brooks, C.L., III. Selectivity in K^+ channels is due to topological control of the permeant ion's coordination state. *Proc. Natl. Acad. Sci. USA* **2007**, *104*, 9260–9265. [CrossRef]
7. Summhammer, J.; Sulyok, G.; Bernroider, G. Quantum Dynamics and Non-Local Effects Behind Ion Transition States during Permeation in Membrane Channel Proteins. *Entropy* **2018**, *20*, 558. [CrossRef]
8. Furini, S.; Domene, C. Atypical mechanism of conduction in potassium channels. *Proc. Natl. Acad. Sci. USA* **2009**, *106*, 16074–16077. [CrossRef] [PubMed]
9. Gwan, J.-F.; Baumgaertner, A. Cooperative transport in a potassium ion channel. *J. Chem. Phys.* **2007**, *127*, 045103. [CrossRef] [PubMed]

10. Koepfer, D.A.; Song, C.; Gruene, T.; Sheldrick, G.M.; Zachariae, U.; de Groot, B.L. Ion permeation in K^+ channels occurs by direct Coulomb knock-on. *Science* **2014**, *346*, 352–355. [CrossRef]
11. Fowler, P.W.; Abad, E.; Beckstein, O.; Sansom, M.S.P. Energetics of multi-ion conduction pathways in potassium ion channels. *J. Chem. Theory Comput.* **2013**, *9*, 5176–5189. [CrossRef]
12. Sansom, M.S.; Shrivastava, I.H.; Bright, J.N.; Tate, J.; Capener, C.E.; Biggin, P.C. Potassium channels: Structures, models, simulations. *Biochim. Biophys. Acta (BBA) Biomembr.* **2002**, *156*, 294–307. [CrossRef]
13. Zhou, Y.; Morais-Cabral, J.H.; Kaufman, A.; MacKinnon, R. Chemistry of ion coordination and hydration revealed by a K^+ channel–Fab complex at 2.0 Å resolution. *Nature* **2001**, *414*, 43–48. [CrossRef] [PubMed]
14. Verlet, L. Computer "Experiments" on Classical Fluids. I. Thermodynamical Properties of Lennard−Jones Molecules. *Phys. Rev.* **1967**, *159*, 98–103. [CrossRef]
15. Ponder, J.W.; Case, D.A. Force Fields for Protein Simulations. *Adv. Protein Chem.* **2003**, *66*, 27–85.
16. Iwamoto, M.; Oiki, S. Counting Ion and Water Molecules in a Streaming File through the Open-Filter Structure of the K Channel. *J. Neurosci.* **2011**, *31*, 12180–12188. [CrossRef]
17. Crank, J.; Nicolson, P. A practical method for numerical evaluation of solutions of partial differential equations of the heat conduction type. *Math. Proc. Camb. Phil. Soc.* **1947**, *43*, 50–67. [CrossRef]
18. Kopec, W.; Rothberg, B.S.; de Groot, B.L. Molecular mechanism of a potassium channel gating through activation gate-selectivity filter coupling. *Nat. Commun.* **2019**, *10*, 5366. [CrossRef]
19. VanDongen, A.M.J. K channel gating by an affinity-switching selectivity filter. *PNAS 101* **2004**, *9*, 3248–3252. [CrossRef]
20. .Summhammer, J.; Sulyok, G.; Bernroider, G.; Cocchi, M. Forces from Lipids and Ionic Diffusion: Probing Lateral Membrane Effects by an Optimized Filter Region of Voltage Dependent K+ Channels (Preprint 2020). Available online: https://www.researchgate.net/publication/339616148_Forces_from_Lipids_and_Ionic_Diffusion_Probing_lateral_membrane_effects_by_an_optimized_filter_region_of_voltage_dependent_K_channels (accessed on 20 June 2020).
21. Schlosshauer, M. Decoherence, the measurement problem, and interpretations of quantum mechanics. *Rev. Mod. Phys.* **2005**, *76*, 1267–1305. [CrossRef]
22. Salari, V.; Moradi, N.; Fazileh, F.; Shahbazi, F. Quantum Decoherence Timescales for Ionic Superposition States in Ion Channels. *arXiv* **2015**, arXiv:1410.7304v1.
23. Salari, V.; Naeij, H.; Shafiee, A. Quantum Interference and Selectivity through Biological Ion Channels. *Sci. Rep.* **2017**, *7*, 4162. [CrossRef] [PubMed]
24. Qaswal, A.B. Magnesium Ions Depolarize the Neuronal Membrane via Quantum Tunneling through the Closed Channels. *Quantum Rep.* **2020**, *2*, 5. [CrossRef]
25. Maris, H.J. Electrons in Liquid Helium. *J. Phys. Soc. Jpn.* **2008**, *77*, 111008. [CrossRef]
26. Berneche, S.; Roux, B. A gate in the selectivity filter of potassium channels. *Structure* **2005**, *13*, 591–600. [CrossRef] [PubMed]
27. Martin, F.; Zipse, H. Charge distribution in the water molecule—A comparison of methods. *J. Comput. Chem.* **2005**, *26*, 97–105. [CrossRef]
28. Ridgeway Scott, L.; Fernandez, A. *A Mathematical Approach to Protein Biophysics*; Springer: Berlin/Heidelberg, Germany, 2017; p. 121.
29. Garofoli, S.; Jordan, P.C. Modelling permeation energetics in the KcsA potassium channel. *Biophys. J.* **2003**, *84*, 2814–2830. [CrossRef]
30. Furini, S.; Domene, C. Computational studies of transport in ion channels using metadynamics. *Biochim. Biophys. Acta* **2016**, *1858*, 1733–1740. [CrossRef]
31. Noskov, S.Y.; Bernéche, S.; Roux, B. Control of ion selectivity in potassium channels by electrostatic and dynamic properties of carbonyl ligands. *Nature* **2004**, *431*, 830–834. [CrossRef]
32. Feenstra, K.A.; Hess, B.; Berendsen, J.C. Improving efficiency of large time-scale molecular dynamics simulations of hydrogen rich systems. *J. Comp. Chem.* **1999**, *20*, 786–798. [CrossRef]
33. Chung, S.H.; Corry, B. Conduction Properties of KcsA Measured Using Brownian Dynamics with Flexible Carbonyl Groups in the Selectivity Filter. *Biophys. J.* **2007**, *93*, 44–53. [CrossRef]